Heliyon 8 (2022) e11030

Contents lists available at ScienceDirect

Heliyon

journal homepage: www.cell.com/heliyon

Review article

Progress in the experimental and computational methods of work function evaluation of materials: A review

O.C. Olawole [a,*], D.K. De [b], O.F. Olawole [c], R. Lamba [d], E.S. Joel [e], S.O. Oyedepo [f], A.A. Ajayi [g], O.A. Adegbite [h], F.I. Ezema [i,j], S. Naghdi [k], T.D. Olawole [l], O.O. Obembe [m,n], K.O. Oguniran [o]

[a] Department of Physics, Covenant University, Ota, Ogun State, Nigeria
[b] Sustainable Green Power Technologies, Mansfield, TX, 76063, USA
[c] Department of Physics, Mountain Top University, Ibafo, Ogun State, Nigeria
[d] Department of Electrical Engineering, Malaviya National Institute of Technology Jaipur, Malaviya Nagar, Jaipur-302017, Rajasthan, India
[e] Department of Earth Sciences, Faculty of Natural, Applied and Health Sciences, Anchor University, Lagos State, Nigeria
[f] Department of Mechanical Engineering, Covenant University, Ota, Ogun State, Nigeria
[g] Department of Mathematical and Physical Sciences, Afe Babalola University, Ado-Ekiti, Nigeria
[h] Department of Chemical Engineering, Covenant University, Ota, Ogun State, Nigeria
[i] Department of Physics and Astronomy, University of Nigeria, Nsukka, Enugu State, Nigeria
[j] Africa Centre of Excellence for Sustainable Power and Energy Development, University of Nigeria, Nsukka, Enugu State, Nigeria
[k] Physikalisch-Technische Bundesanstalt, Abbestr. 2-12, 10587 Berlin, Germany
[l] Department of Biochemistry, Covenant University, Ota, Ogun State, Nigeria
[m] Department of Biological Sciences, Covenant University, Ota, Ogun State, Nigeria
[n] UNESCO Chair on Plant Biotechnology, Plant Science Research Cluster, Department of Biological Sciences, Covenant University, Ota, Ogun State, Nigeria
[o] Department of Chemistry and Biochemistry, Caleb University, Imota, Ogun State, Nigeria

ARTICLE INFO

Keywords:
Work function
Energy
Model
Material
Electron
Metal
DFT

ABSTRACT

The work function, which determines the behaviour of electrons in a material, remains a crucial factor in surface science to understand the corrosion rates and interfacial engineering in making photosensitive and electron-emitting devices. The present article reviews the various experimental methods and theoretical models employed for work function measurement along with their merits and demerits are discussed. Reports from the existing methods of work function measurements that Kelvin probe force microscopy (KPFM) is the most suitable measurement technique over other experimental methods. It has been observed from the literature that the computational methods that are capable of predicting the work functions of different metals have a higher computational cost. However, the stabilized Jellium model (SJM) has the potential to predict the work function of transition metals, simple metals, rare-earth metals and inner transition metals. The metallic plasma model (MPM) can predict polycrystalline metals, while the density functional theory (DFT) is a versatile tool for predicting the lowest and highest work function of the material with higher computational cost. The high-throughput density functional theory and machine learning (HTDFTML) tools are suitable for predicting the lowest and highest work functions of extreme material surfaces with cheaper computational cost. The combined Bayesian machine learning and first principle (CBMLFP) is suitable for predicting the lowest and highest work functions of the materials with a very low computational cost. Conclusively, HTDFTML and CBMLFP should be used to explore the work functions and surface energy in complex materials.

1. Introduction

The work function, according to the scientists of the twentieth century (fundamental property of material's surface) is the minimum energy required to extract an electron from a material surface [1, 2, 3, 4, 5, 6]. Its dependence on physical factors such as temperature, surface dipole, doping, and electric field cannot be underestimated as investigated by the authors of the twentieth century [7, 8, 9, 10] that

* Corresponding author.
E-mail address: olukunle.olawole@covenantuniversity.edu.ng (O.C. Olawole).

https://doi.org/10.1016/j.heliyon.2022.e11030
Received 31 March 2022; Received in revised form 16 August 2022; Accepted 6 October 2022

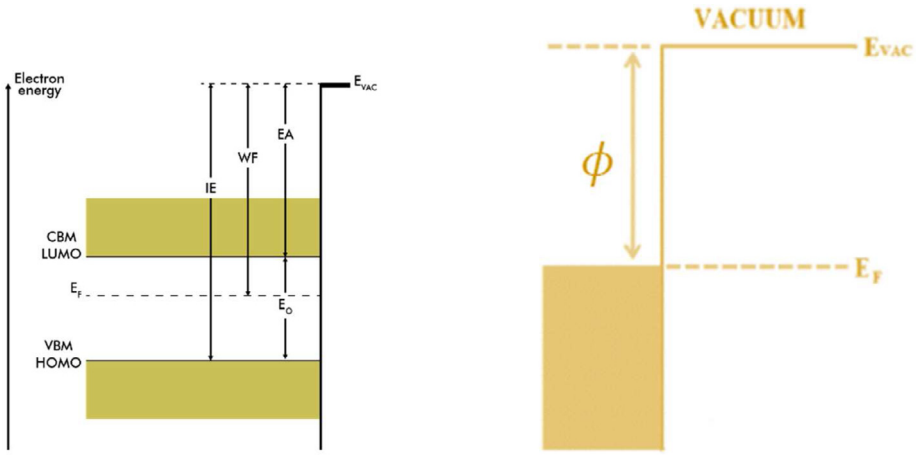

Fig. 1. (a) Energy profile of a semiconductor and (b) work function of a metal.

image potential contributes to the work function of materials and this work function depends on temperature [11, 12, 13, 14, 15, 16]. Also, experimental and theoretical findings revealed that work function is dependent on electronic heat capacity[17], thermal expansion of the lattice[17], Young's modulus [17, 18, 19], friction [20], adhesion [21] surface energy [22], fracture toughness[19, 20, 23], corrosion [15, 21, 24], and yield strength and hardness [26].

This work function remains a governing factor of the band alignment in semiconductors [27] and an essential property of metal-semiconductor contact quality [28, 29] in the development of new carbon/graphene-based devices such as graphene transistors [30, 31], carbon-nanotubes [31, 32], gas nanosensors [33], and electronic metallurgy [35]. Also, a twenty-first-century scholar [34] revealed that the behaviour of ions, atoms and molecules inside solid materials are governed by work function (ϕ) [11, 26] and some other key factors such as vacuum level (E_{VAC}), Fermi level (E_F), energy bandgap (E_G), electron affinity (EA) and ionization energy (IE), as shown in Fig. 1(a-b). Consequently, E_G is defined as the energy difference between the conduction band and valence band [36] while E_{VAC} is the local vacuum level [37]. In addition, EA is the amount of energy released when an additional electron is added to a neutral atom or molecule [25, 27]. However, IE in Fig. 1 depicts the minimum energy required for removing an electron out of a neutral atom or molecule in its ground state [34]. E_F defines the energy up to which electrons occupy all energy states of metal at absolute zero temperature [36]. Also, the work function in Eq. (1) typifies the difference between the Fermi level and the vacuum level, as depicted in Fig. 1b. In Fig. 1 [34], CBM denotes the conduction band minimum (CBM), and VBM denotes the valence-band maximum (VBM) through which electron and hole transit in an inorganic semiconductor. LUMO is the lowest unoccupied molecular orbitals (LUMO), and HOMO is the highest occupied molecular orbitals (HOMO) which are energy levels through which the electron and hole migrate in a semiconductor.

$$\phi = E_{VAC} - E_F \tag{1}$$

Arguably, materials with a lower work function that operate at a lower temperature are noted to release more electrons [29, 30]. Consequently, the work function is of tremendous technological importance in many applications such as thermionic energy converters [31, 32], printed and organic electronics [42, 43, 44], emerging perovskite solar cells technology fluorescent light tube [45], electron emission gadgets (terahertz sources) [46, 47], scientific instruments that use electron sources [30, 39, 40, 41, 50], catalysis [42, 43, 51, 52], electrochemistry [53, 54, 55], corrosion resistance [25, 56, 57] and as an interfacial diagnostic tool in material [58]. These novel applications are realizable if the materials are mechanically, chemically and thermally stable (thoriated tungsten and lanthanum hexaboride), preferably caesiated metals of low work function [48, 49, 59, 60], as applied in thermionic energy converter [38, 61, 62, 63, 64].

Furthermore, unusual result happens when adsorption and desorption kinetics [65, 66] takes place on the host (material) surface as recorded in the desorption of xenon on the homogeneous surfaces of palladium $Pd(110)$, $Pd(100)$, and $Pd(111)$ [67]. Interestingly, $Pd(110)$, $Pd(100)$ have the same packing density of $5.73 \times 10^{14} Xe/\text{cm}^2$ as against $Pd(111)$ with different packing density of $5.09 \times 10^{14} Xe/\text{cm}^2$. Also, the sticking coefficient differs in the three Pd surfaces such that $Pd(110)$ has one dimensional sticking coefficient with Xenon atom found on the lattice trough. $Pd(100)$ face has a zero sticking coefficient, while Xe atoms have a total sticking coefficient (sitting in the threefold hollow sites) on $Pd(111)$ face [67]. Another study of desorption of Tellurium (Te) on W(100) resulted in three distinct binding states on the homogeneous surface [68]. Since the work function of a material is extremely sensitive to the quality of the surface (environmental factor) that causes it. Also, an in-depth understanding of the effects of the environment on the quality of work function measurements is required. Moreover, high spatial resolution measurements are needed for the modern technology-based smaller devices to characterise the complex heterogeneities and homogeneities in the materials used in the microelectronics nanoscience scales.

2. Homogeneous and heterogeneous surfaces

Homogeneous surfaces are formed by interacting monocrystalline films and monocrystalline solids such that its work function contrast $\Delta\phi^*$ between the work function of positive ion, ϕ^+ and negative ion, ϕ^- must be equal to zero electron-volt ($\Delta\phi^* = \phi^+ - \phi^- = 0.0$ eV). Kawano [69] opined that the entire surface of a monocrystalline specimen $W(1\ 1\ 0)$ is homogeneous when it is free of systemic errors which means its degree of monocrystallization $(\delta_m) = 100\%$ and $\Delta\phi^* = 0.00$ eV. Heterogeneous surfaces are formed by surface patches (bumpy and defective) that are interacting electrostatically when their neighbouring surfaces of different work functions are next to each other. Cerofolini and Fondi [70] proposed a model that describes the electron emission from heterogeneous surfaces (single-crystal comprises numerous emitting faces, polycrystalline films, and polycrystalline solids) of metals that are created by a group of isolating homogeneous zones. Each homogeneous patch has a constant work function. The analytical models

Table 1. The work functions of heterogeneous solid metal surfaces for different emission phenomena.

Emission Phenomena	Work Function Expression
Photoemission	$\varphi_a(E) = \int_0^{+\infty} k_B^2 T^2 \frac{\partial^3}{\partial E^3} F\left(\frac{E-\Phi}{k_B T}\right) \varphi(\Phi)\, d\Phi$
Thermionic emission	$\varphi(\Phi) = \frac{1}{2\pi i} \int_{\varepsilon-i\infty}^{\varepsilon+i\infty} \exp(\beta\Phi)\, \bar{y}(\beta)\, d\beta$
Field emission	$\psi(\xi) = \int_{\varepsilon-i\infty}^{\varepsilon+i\infty} \exp(\zeta\xi)\, \chi(\zeta)\, d\zeta$ where, $\psi(\xi) = 2\varphi\left(\xi^{2/3}\right)/3\xi$, $\zeta = b/F$ and $\xi = \Phi^{3/2}$

representing the work function distribution on the surface of heterogeneous surfaces for thermionic emission, photoemission and field emission phenomena were developed by Cerofolini and Fondi [70]. The work function of heterogeneous surfaces varies significantly from one face to another. The work function (in eV) of different faces of tungsten (b.c.c. lattice) is varying greatly with crystal faces-(100), (110), (011), (111), (112) and (116) is given as 4.64, 5.05, 4.53, 4.39, 4.73 and 4.39 eV respectively [71, 72, 73]. The emission from heterogeneous solid metal surfaces can be categorized as photoemission, field emission, and thermionic emission depending upon the energy source, which are briefly defined as follows:

Photoemission: In photoemission, the input energy is the photons/light energy. The photons, incident on the metal surface having energy greater than the work function of the metal causes the electrons to be emitted out from the metal surface.

Thermionic emission: In thermionic emission, the input energy source is the heat/thermal energy. When a metal is heated up to a sufficiently high temperature of order of 2000 °C or more, the electrons are emitted out from the metal surface. The electron emission depends on the temperature of the input heat.

Field emission: In field emission, the input energy source is the strong electric field. When a sufficiently high electric field is applied to a metal surface, the electrons are emitted out from the metal surface. The electron emission is proportional to applied electric field.

The mathematical models describing the work function distribution on the metal surfaces for different emission phenomena are given in Table 1. The detailed derivations of finding the expressions of work functions of heterogeneous surfaces for these three different emission phenomena are given in Appendix A [62]. It is found that a same law cannot be applied to both a heterogeneous surface and a homogeneous surface.

3. Determination of work function

The measurement of the work function of materials with spatially resolved and good reliability is the main barrier in surface characterization for advanced technological applications [74]. The work functions measurement techniques of materials can be broadly classified into two categories. The first category is based on the electron emission process, and the work function is measured on an absolute scale. The material's surface is simulated using different methods such as thermal emission (thermionic emission), photoemission (ultraviolet photoelectron spectroscopy (UPS) and photoelectric effect), field emission (applied electric field) or a combination of these methods. The second category measures the work function differences between various metals (Kelvin probe force microscopy (KPFM)) or during surface modifications similar to adsorption processes. The measurement of work functions using these techniques is relative and generally requires the standard reference work function calculation. Therefore, experimental protocols, including techniques from both categories, are usually needed for measuring work function with good reliability. This study divides the determination of a material's work function into experimental and computational methods.

4. Experimental method

The commonly used experimental techniques for work function determination are photoelectric measurements, ultraviolet photoelectron spectroscopy (UPS), and thermionic emission (Fig. 2), while the work function differences-based techniques for work function determination are contact potential difference (Kelvin probe force microscopy (KPFM), Fig. 3), vibrating capacitor (Zissman method), and diode methods.

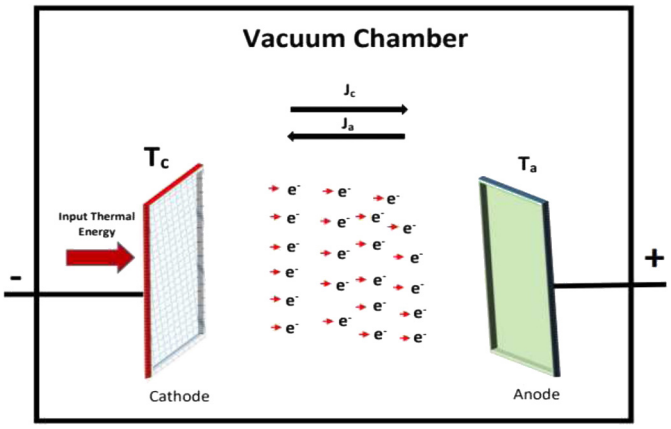

Fig. 2. Schematic diagram of the thermionic electron emission from a thermionic energy converter. T_c is cathode temperature, and T_a is anode temperature J_c and J_a are the current flow from cathode to anode and from anode to cathode, respectively.

Among the various characterization techniques for work function measurements of different materials, KPFM and x-ray photo electron emission microscopy (XPEEM) are the most promising and powerful work function measurements with high spatial resolution and reliability. However, Table 2 shows the experimental findings of various authors on the work function of materials.

5. Computational methods

Table 3 reviews some of the scholarly models adopted by theorists in fitting the work functions of reliable experimental data.

6. Conclusion

The review summarizes the various experimental techniques and computational models for measuring the work function of different materials. Although, desorption methods, both as a single method and as a combined technique with other procedures such as flash desorption and infrared spectroscopy, have been adopted to interpret the mechanism of materials' surface reaction. The other most widely used electron emission-based techniques (photoelectric measurements, UPS, thermionic emission) and the work function differences-based techniques (contact potential difference [the KPFM], vibrating capacitor [Zissman method] and diode methods) for measurement of work function have been discussed. The work function distribution of homogeneous and heterogeneous surfaces has also been discussed in brief. The review also reveals that KPFM and XPEEM are the most promising, accurate, reliable, and powerful techniques for work functions measurement. Moreover, it has been observed that the metallic plasma model can predict the work functions of simple transition, inner transition and rare-earth metals as compared to the other models. However, the stabilized Jellium model (SJM) has the potential to predict the work functions of transition metals, simple metals, rare-earth metals and inner transition metals. The metallic plasma model (MPM) can predict the work functions of the polycrystalline metals. Also, the study showed that the density functional theory (DFT) is suitable modelling method for predicting the lowest and highest work functions of the materials, but with a higher computational cost. The high-throughput density functional theory and machine learning (HTDFTML) tools are suitable for predicting the lowest and highest work functions of extreme materials surfaces with cheaper computational cost.

Table 2. Summary of Experimental measurement of materials' work function.

Technique	Principle/Governing Equation	Measurement	Defect	Merits	Demerits	Findings
KPFM	Atomic force microscopy $W_s = W_{tip} - eV_{dc}$	Work function (WF) is obtained from the potential difference between the tip of the cantilever and the sample.	It is highly suitable for 2D transition metal dichalcogenide (TMD) materials [76].	It is helpful to obtain the electronic state, composition, and homogeneity of the sample. It has excellent spatial resolution and energy sensitivity.	KPFM is affected by humidity (environmental factor).	It can measure the work function of metals, semiconductors, and nanomaterials with all accuracy up to 10 meV with a spatial resolution of around 10 nm.
Ultra-violet photoelectron spectroscopy (UPS)	Photon-excited charge emission process $W_s = h\upsilon - (E_F - E_{cutoff})$	UPS measures the kinetic energy spectra of the emitted photoelectrons.	partially suitable	UPS gives relatively results of the WF.	UPS is prone to surface contamination. It is only perform in a vacuum (At ambient conditions there is a lack of information of the material's work function) [76].	Work function is obtained from the subtraction of the width of the photoelectron spectrum from the photon energy of the excitation light.
Thermionic emission (TE)	Thermally excited charge emission process $W_s = k_B T log\left(J/A_0 T^2\right)$	TE determines the WF from Richardson Dushman of Equation (3).	Not suitable	Removal of sample surface's adsorbent at high temperature.	TE is affected by space charge, a higher work function of the cathode and a few materials that can withstand the temperature of 2000 K.	Existence of a linear relationship between current density and work function of the sample.
Field electron Emission (FE)	Electrostatic-excited charge emission $W_s = k_B T log\left(J/A_r T^2\right)$	FE determines the WF from Fowler-Nordheim of Equation (4).	Not Suitable	FE gives more detailed information about the bulk than the surface of the materials.	FE measures the bulk materials. Susceptible to contamination of the emitter surface.	A linear relationship between current density and work function of the sample.
Photoemission electron microscopy (PEEM)	Generation of image contrast through local variation in electron emission.	WF is determined from secondary electron emission spectra.	partially suitable for material	PEEM enhances lateral resolution but eliminates topographic effects in samples.	Energy sources for PEEM such as synchrotron radiation, X-ray radiation and ultra-violet could result in health complications if not well handled. It cannot detect defect at spatial resolution of >1 μm and energy resolution of >400 meV. PEEM with spatial resolution of 20 nm is quite expensive [77].	PEEM is a suitable method for flat and smooth surface sample with a spatial resolution of around 1 μm and energy resolution of around 400 meV [78].
Internal photoemission spectroscopy (IPES)	Modification of Fowler's theory	WF is found from the spectral onset of electron or hole photoemission from one solid into another Barrier and bandgap measurement.		IPES is reliable and straightforward to use.	An error occurs when the sample is not perpendicular to the electron detector. Disagreement in literature overwork function due to IPES Sensitivity nature to any subtle changes in the experimental conditions.	IPES is suitable to determine the work function of samples such as insulators, metals semiconductors and nanomaterials [79, 80].
Low energy electron microscopy (LEEM)	Strong elastic scattering of low energy electrons. It uses the combination of high resolutions imaging and high sensitivity from local electrostatic potentials.	Quantification of local WF differences.		It provides a high lateral resolution. It uses low energy to image the surface of the sample.	Difficulty in interpreting samples that contain different areas of work function.	A suitable method to probe the work function of a sample.
Scanning tunnelling microscopy (STM)	Vacuum tunnelling	Measuring the current through the tip of the scanning tunnelling microscope as a function of the distance.	Partially suitable	Determination of work function on the atomic scale.	STM has low throughput and limited field of view.	It has a great potential to study the local work function of graphene on Ir(111) [81].
Capacitance-voltage (C-V)	Sweeping the applied voltage from accumulation to inversion. Also, from inversion to accumulation.	Both capacitance-voltage on terraced oxide structure and current-current (J-V) on barrier height was used to examine the effective work functions of the structures.		Both C-V and J-V are suitable for predicting the practical work function of the material.	C-V is not suitable for the actual work function of the material.	C-V is suitable for measuring the effective work function of terraced oxide structure, while J-V is suitable for measuring the actual work function of the system [82].
Contact potential difference (CPD) (Kelvin method and Diode method)	Usually gold is used as a reference electrode.	Examine the adsorption of molecule surfaces and modify mono crystal surface.		Applicable to insulator as in the case of Kelvin probe method [83]. Concise experimental set-up (diode method [84, 85]).	Work function significantly relies on tip condition. It does not work effectively for immersed specimen.	Applicable in corrosion science electrochemical use for electrodes just covered by ultra-thin electrolyte layers [86].

Table 3. Various models for predicting the work function of metals.

Number of Metals	Model	Contribution	Merit	Demerit	Error (%)
14	Adoption of uniform background charge (instead of the lattice of ions) with exchange and correlations effects.	Only nine elements out of fourteen slightly modelled the experimental values correctly [26].	Simple pseudopotential model is suitable for simple metals.	Model not suitable for metals in s-d bands.	Simple metals have 5-10%, while noble metals have 15-30%.
26	The authors applied the hydrodynamic model of Bloch and Tomas-Fermi approximation.	They were reasonable agreement among numerical values, experimental results, and theoretical prediction for the examined metals [87].	It is suitable for the numerical value of the integral at 0.4.	It is not suitable for the numerical value of the integral at 0.5. The model only considered the contribution of free electrons to the work function.	-
32	Utilization of a purely electrostatic approach	They used the Mathesis construct (overlapping spherical atomic charge-density approximation and chemical potential) to fit the experimental data [88].	It models relationship between dipole barrier of nopolar crystal and the moment of the spherical densities of metals.	The model is not suitable for metals surface calculations.	80%
5	Thomas-Fermi Von Weizsäcker method to solve the slab geometry jellium model for five alkali metals and Pseudojellium model for four metals.	The Jellium model fitted the experimental data (Smith [89]) well than the Pseudojellium model (Lang and Kohn [90].	It is useful for calculating the electronic properties of alkali-metal slabs.	The model is not useful for the electronic properties of other metal slabs.	6% (Jellium model) and 15% (Pseudojellium model).
1	Modelling work function as a function of electron density parameter within the local-density approximation.	Model predicted the low, metallic and high bulk electron densities [91].	Model is useful for predicting work functions of low, and metallic bulk electron densities.	Model is not suitable for higher bulk electron densities. It noted the collapsed of Jellium model for highly-non-uniform bulk densities.	-
12	Structure-less pseudo-potential model	They modelled work function dependence on electron density parameters. The study also corrected the anomalies of Jellium model [92].	The model is appropriate to study the interfaces, metallic clusters, vacancies, and the electromagnetic response of materials.	It is not suitable for high density metals.	-
17	Improved ideal electron gas model	They found that the surface energies of the model reduce by 25%, and the work functions were more significant by 15% compared with the experiment. In addition, the failure of the Jellium theory made them apply the pseudojellium model in the absence of external force. And their study found a work function of 0.3 eV above the experimental value for both low and medium electron density. The surface energy is at $r_s = 1.6$ a.u. and disintegrates for high densities [93].	It can be used to predict the work functions of simple metals.	It not suitable for complex metals.	-
40	Green's function technique is based on the linear muffin-tin orbitals together with tight-binding.	They found a model that could physical. Described the surface phenomena of the materials [94].	Abinitio model accurately predicted the monovalent, divalent, polycrystalline metals and trivalent of non-transition metals with experimental values.	It is not suitable for 5d elements.	15%
9	Density functional theory	The study disapproved relationship between surface energy and cohesive force in that contributions of orbital structure, polarization, and free atom spin are needless in surface phenomena [95].	It is suitable for calculating the surface energy and work function of low index surfaces of 4d transition metals.	Computationally expensive	
2	Jellium slab model	The study found how the variations of the Fermi wavelength are dependent on the thickness of a crystalline slab [96].	It is appropriate for the calculation of nanomaterial work function.	It is not applicable to the work function of macro material.	-
1	Thin slab/Jellium slab model	The model determined precisely the work function of Aluminum (Al) and also showed how quantum side effect could be reduced [97].	It is suitable for Al.	The model only applicable to one element and not all metals.	-

(*continued on next page*)

Table 3 (*continued*)

Number of Metals	Model	Contribution	Merit	Demerit	Error (%)
59	Abinitio models	The relationship the among the work function, the Fermi energy and the electron density made the model to establish better agreement with experimental for metals and semimetals [98].	It is suitable for metals and semimetals.	The models are not suitable for semiconductors.	8-12%
	Classical electrodynamics model	Study found emission process of microscopic surface structure of metals, and provided justification for continuous decoherence from quantum to classical states [99].	It is used to model the work function of metals and the optimum work functions for single layers of electropositive elements on metal substrates.	The model cannot predict the effective mass of the escaping electron with orientation within the crystal.	-
29	Phenomenological model	Classical electrodynamic models fitted the experimental data far better than Abinitio [100].	The models can probe the work function of metals, transition metals, lanthanides, and actinides accurately.	It cannot be used to upgrade the Abinitio model.	-
3	Application of repeated charged slabs in density functional theory (DFT)	Charged slab model was in good agreement with the conventional density functional theory for $Al(100)$, $Si(111)$ and $TiO_2(110)$ [101].	It provides total energies of charged surface systems.	The model is only applicable to three elements. It requires large vacuum thickness.	2-3%
3	Slab model and first principle electronic structure calculation	The study showed that the work function of noble metals is dependent on surface orientation [102].	The model is only useful for rough prediction of noble metals.	It breaks down in Smoluchowski law.	
20	DFT	The study found that the bulk O 2*p*-band centre could serve as a semi-quantitative descriptor of the work function for both AO- and BO_2-terminated (001) perovskite surfaces [103].	It is used to search for a novel, low work function material specifically in electron emission applications. It is useful for high work function material.	High computational cost.	-
3	DFT	The authors found out that work function is dependent on surface termination, surface reconstructions, oxygen vacancies, and Hetero-structuring [104].	It serves as reference values for the *tunability* of work functions.	Lack of experimental data to judge the predicted data points.	-
73	DFT	The applied local density approximation (LDA) and the Perdew-Burke-Ernzerhof parametrization of the generalized gradient approximation (PBE-GGA) functional to probe the surface energy and work function of materials [105].	Both LDA and PBE-GGA functional are good for the prediction of the material work function. LDA can predict surface energy correctly.	PBE-GGA can not be used to predict surface energy of a material. Higher computational cost.	<3 eV
10	DFT	Study found out that stable Ba-O adsorbates less than unity are suitable surfaces for thermionic cathode. Each passivated dangling bond of tungsten was thermodynamically favoured with a single O atom, and Ba that resulted into $Ba_{0.125}O$ or $Ba_{0.125}O$ [106].	It is used as Cs-coated metal for thermionic energy converter.	It is not applicable to one polycrystalline metal. Adsorption of Ba and O are not considered for pits, ledges, and surface steps polycrystalline W. High computational cost.	-
9	DFT used in Vienna ab initio Simulation Package (VASP) with PBE functional	The study found a strong correlation between the **2*p*** band centres and work functions that depicted the volcano plot [107].	It is used to benchmark the lowest work function a material can attain.	It is only applicable to 2d materials.	-
5	Semi-empirical equation (modern use of Schrodinger equation)	Semi-empirical equation predicted the work functions Li, Na, K, Rb very well with the experimental. Experimental value of Caesium 2.14 eV was doubted [108].	It gave higher accuracy in the absence of computer programme and extra parameters.	The method was not tested for all the metals.	2-3%
7	Unconventional quantum model	The study found the analytical equations for the permitted single- electron energy states in the real metal and the energy of the system N interacting electrons. It also applied mechanical parameters of metals to modify the function of the density of states [109].	It is suitable for alkali metals. It is also used to calculate the electron chemical potential of alkali metals.	The method is not suitable to calculate the chemical potentials of metals because of negative results.	-

Table 3 (*continued*)

Number of Metals	Model	Contribution	Merit	Demerit	Error (%)
1	DFT	[110]	The Scandium (Sc) is a suitable material for tuning O chemical potential in high-emission Sc-containing cathode.		-
1	First Principles	They observed the absolute work functions and electron affinities of bulk $SrNb_{0.01}Ti_{0.99}O_3$ (001) terminated along the TiO_2 and SrO planes [111].	It reveals how defects increase the work function of the materials. Increment of negative charge density on the surface.	Limited to two terminations.	-
72	Wulff shape model for weighted work function	The authors built a largest database for anisotropic work functions. Also, they examined the simple bond breaking rules for metallic systems with numerous maximum Miller index [112].	It is useful for probing a more generalized work function anisotropy.	The database is only for polycrystalline specimens.	0.2 eV
1	DFT	It validated the result of STEM for 2D TMDs [76].	It connects the work function variance and the defect density of heterogeneity materials with high spatial resolution and energy sensitivity.	-	-
25	Double Dipole Model	The study discovered that work function remained unchanged because the chemical potential is not dependent on temperature. It also found out that work function experienced changes because dipole layer of the metal was temperature dependent [113].	It helps in determining the work function of twenty-five metals.	It is not applicable to all metals.	-
1	DFT with Heyd–Scuseria–Ernzerhof (HSE)	They model when compare with available experimental data could predict accurately the work function values of clean and reconstructed $SrTiO_3$ surfaces [114].	It models oxide material of $SrTiO_3$ very well.	The model has not be tested on other oxides materials.	0.2 eV
10	Machine Learning Approach (Combination of Bayesian Machine Learning and First-Principles Calculation)	This model successfully predicts the work functions of the top lowest and top highest materials [115].	The model can predict higher or lower work functions of numerous metals including a lanthanide alkali, and alkaline earth metal. The model used bulk calculation. Low computational cost.	The model ignored the work functions relationship with their surfaces.	-
59	Metallic plasma model (MPM) and stabilised jellium model (SJM)	Results of MPM [116] were compared with stabilised jellium model (SJM), ab initio model and experimental values [116]. MPM predicted the experimental well SJM [92] was in good agreement with experimental data for the transition metals, simple metals, rare-earth metals and inner transition metals [116].	MPM is suitable for pure metals and polycrystalline metals. MPM is suitable for non-metals.	Abinitio model only fitted the experimental values of Ba, Ca and Sr well and failed to predict all other metals. SJM is not suitable for non-metals.	-
29270	high-throughput density functional theory and machine learning	The model achieve the same accuracy as DFT but with a greater computational speed that is 10^5 times faster than DFT [117].	The model can predict material surfaces with both extreme low and high work functions. Low computational cost.	The model has not been tested for materials with relaxed surfaces. The model has not considered surface energy as to which surface termination is most stable.	0.19 eV
15	DFT	The study found $(La,\ Ba)B_6$ suitable because of its lower work function over LaB_6 and BaB_6 [118].	It suitable to find the work function of hexaboride, tetraborides, and transition metal nitrides.	The model will not be suitable at the presence of vacancy defects.	-

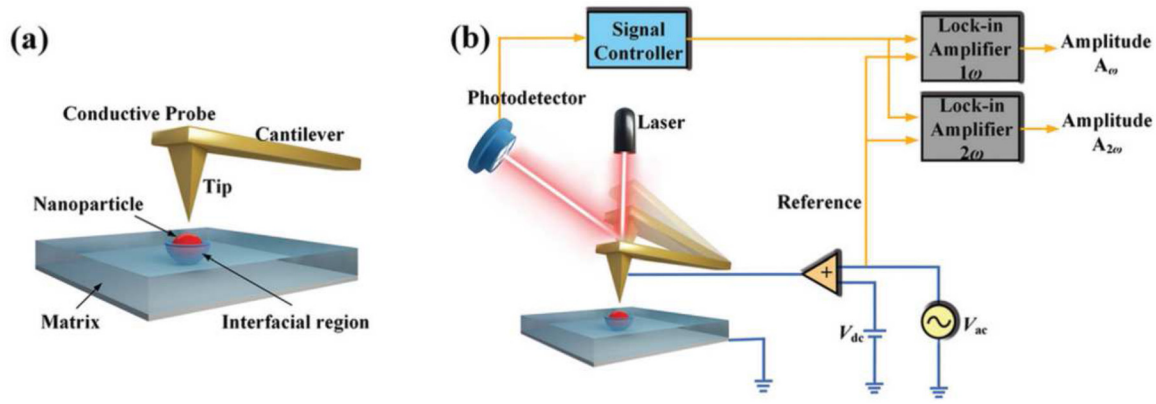

Fig. 3. (a) Schematic diagram of KPFM, and (b) its working principle. (Reprinted from Luo et al. [75] Copyrights (2019), with permission from the Royal Society of Chemistry.)

This study suggests that the HTDFTML and CBMLFP models should be explored in more detail in future to determine the work functions and surface energy (finding surface termination that provides higher stability) of the complex metals in relation to their surface phenomena in terms of grain boundaries formation, catalytic behaviour, surface segregation, adsorption, growth rate, sintering and the formation of the crystallites. Further, the surface relaxation should be included in both HTDFTML and CBMLFP computations in order to get work functions of relaxed surfaces. Lastly, temperature-dependent work function models may be helpful in exploring new materials

Declarations

Author contribution statement

All authors listed have significantly contributed to the development and the writing of this article.

Funding statement

This research did not receive any specific grant from funding agencies in the public, commercial, or not-for-profit sectors.

Data availability statement

No data was used for the research described in the article.

Declaration of interests statement

The authors declare no conflict of interest.

Additional information

No additional information is available for this paper.

Acknowledgements

The authors gratefully appreciate the facilities and financial support provided by Covenant University Centre for Research, Innovation and Development (CUCRID), and Covenant University to carry out the reported research work.

Appendix A

The heterogeneous surface is formed by a set of homogeneous patches having their respective work function as Φ_i. The average current density emitted from heterogeneous surface is given as [70]:

$$j(X) = \sum_i J\left(X, \Phi_i\right) \varphi\left(\Phi_i\right) \tag{1a}$$

where, $J\left(X, \Phi_i\right)$ is the current density emitted from the patch with work function, Φ_i and X is the photon energy (E), temperature, (T) and electric field, (F) in the photoemission, thermo-emission and field emission respectively. Eq. (1) is true when each patch is emitting independently and there is no lateral interaction among the patches. However, for the heterogeneous surface, the continuum limit of Eq. (1a) can be considered as:

$$j(X) = \int_0^{+\infty} J(X, \Phi)\, \varphi(\Phi)\, d\Phi \tag{2a}$$

where, $\varphi(\Phi)\, d\Phi$ is the surface fraction having work function between Φ and $\Phi + d\Phi$.

Eq. (2a) is valid when the following hypotheses are strictly valid-the surface is formed by a set of homogeneous patches, each having a work function, Φ_i and there is no laterally interaction in the patches.

Since $J\left(X, \Phi_i\right)$ is theoretically known using the different emission laws and $j(X)$ is experimentally known, then the distribution function, $\varphi(\Phi)$ can be determined. The function, $j(X)$ is different for a homogeneous and heterogeneous surfaces.

Now, by considering, $j(X) = J\left(X, \overline{\Phi}\right)$, Eq. (2a) can be written as:

$$J\left(X, \overline{\Phi}\right) = \int_0^{+\infty} J(X, \Phi)\, \varphi(\Phi)\, d\Phi \tag{3a}$$

Eq. (3a) is satisfied if $\varphi(\Phi) = \delta\left(\Phi - \overline{\Phi}\right)$ which means the surface must be homogeneous. The function, $\varphi(\Phi)$ must satisfy the following normalized condition:

$$\int_0^{+\infty} \varphi(\Phi)\, d\Phi = 1$$

A.1. Photoemission

The Fowler [119] theory of photoemission is modified by the Du Bridge [120] and it is called as Fowler-Du Bridge theory which is stated as:

$$J(E, \Phi) = BIk_B^2 T^2 F\left(\frac{E - \Phi}{k_B T}\right) \tag{4a}$$

where I the light intensity, B is a characteristic constant, independent of E and Φ, and k is the Boltzmann constant.

The average current density emitted from heterogeneous surface (given in Eq. (2a)) in case of photoemission phenomena is given as:

$$j(E) = \int_0^{+\infty} BIk_B^2T^2F\left(\frac{E-\Phi}{k_BT}\right)\varphi(\Phi)\,d\Phi \tag{5a}$$

Eq. (4a) can also be expressed as conditionally:

$$J_a(E,\Phi) = \begin{cases} 0 & E < \Phi, \\ \frac{1}{2}BI(E-\Phi)^2 & E \geq \Phi \end{cases} \tag{6a}$$

Substituting Eq. (6a) into (5a), the average current density emitted from heterogeneous surface in photoemission is given as:

$$j(E) = \frac{1}{2}BI\int_0^E (E-\Phi)^2\,\varphi_a(\Phi)\,d\Phi \tag{7a}$$

The solution of Eq. (7a) which gives the approximate work function distribution is given as:

$$\varphi_a(E) = \frac{1}{BI}\frac{d^3j(E)}{dE^3} \tag{8a}$$

Now, to check accuracy of Eq. (8a), the differentiation of Eq. (5a) three times with respect to E is given as:

$$\frac{d^3j(E)}{dE^3} = BI\int_0^{+\infty} k_B^2T^2\frac{\partial^3}{\partial E^3}F\left(\frac{E-\Phi}{k_BT}\right)\varphi(\Phi)\,d\Phi \tag{9a}$$

Substituting Eq. (9a) into Eq. (8a) results in:

$$\varphi_a(E) = \int_0^{+\infty} k_B^2T^2\frac{\partial^3}{\partial E^3}F\left(\frac{E-\Phi}{k_BT}\right)\varphi(\Phi)\,d\Phi \tag{10a}$$

where, subscript 'a' represents the approximation value.

The identity is given as

$$\Phi(E) = \int_0^{+\infty} \delta(E-\Phi)\,\varphi(\Phi)\,d\Phi \tag{11a}$$

The comparison of Eq. (10a) with the identity given by Eq. (11a) represents that the approximate work function distribution, $\varphi_a(E)$ is exactly similar to the exact one $\Phi(E)$. In photoemission phenomena, the method used for evaluating the quality of approximation has a general validity and the relation given by Eq. (12a) must be found for evaluating the validity of the method.

$$\varphi_a(E) = \int_o^{+\infty} H(E,\Phi)\,\varphi(\Phi)\,d\Phi \tag{12a}$$

where, $H(E,\Phi)$ is a kernel that depends on the used approximation. Comparison of Eq. (12a) and Eq. (11a) reflects that the more $H(E,\Phi)$ resembles $\delta(E-\Phi)$, the more the method is correct.

A.2. Thermionic emission

According to the Richardson law, the thermionic emission from each homogeneous patch at temperature, T is given as:

$$J(T,\Phi) = AT^2\exp\left(-\frac{\Phi}{k_bT}\right) \tag{13a}$$

where A is a universal constant or it may depend on the potential barrier form. It is assumed here that A does not depend on E and Φ.

The average current density emitted from heterogeneous surface (given in Eq. (2a)) in case of thermionic emission phenomena is given as:

$$j(T) = AT^2\int_0^{+\infty}\exp\left(-\frac{\Phi}{k_bT}\right)\varphi(\Phi)\,d\Phi \tag{14a}$$

By substituting, $\beta = \frac{1}{k_bT}$ $\tilde{y}(\beta) = k_b^2\beta^2\tilde{j}(\beta)/A$ and $\tilde{j}(\beta) = j(T(\beta))$ in Eq. (14a) results in the following expression:

$$\tilde{y}(\beta) = \int_0^{+\infty}\exp(-\beta\Phi)\,\varphi(\Phi)\,d\Phi \tag{15a}$$

It is clear from Eq. (15a) that the left hand side function, $\tilde{y}(\beta)$ is the Laplace transform of the work function distribution, $\varphi(\Phi)$ with respect to β and it is strictly related to the experimentally known function, $j(T)$.

The inverse Laplace transform of Eq. (15a) gives the exact solution which is gives as:

$$\varphi(\Phi) = \frac{1}{2\pi i}\int_{\varepsilon-i\infty}^{\varepsilon+i\infty}\exp(\beta\Phi)\,\tilde{y}(\beta)\,d\beta \tag{16a}$$

The Laplace transform converges at a point, ε which is point of the real positive semi-axis.

A.3. Field emission

The field emitted current density for a homogeneous surface emitting at 0 K, is function of field strength, F and work function Φ which is given by the Fowler-Nordheim theory as follows:

$$J(F,\Phi) = a\frac{F^2}{\Phi}\exp\left(-\frac{b\Phi^{3/2}}{F}\right) \tag{17a}$$

where a and b are considered constants which are very slowly varying functions of $F^{1/2}/\Phi$.

The average current density emitted from heterogeneous surface (given in Eq. (2a)) in case of field emission phenomena is given as:

$$j(F) = \int_0^{+\infty} a\frac{F^2}{\Phi}\exp\left(-\frac{b\Phi^{3/2}}{F}\right)\varphi(\Phi)\,d\Phi \tag{18a}$$

After substituting $\zeta = b/F$ and $\xi = \Phi^{3/2}$ in Eq. (18a) and simplifying it results in:

$$\chi(\zeta) = \int_0^{+\infty}\exp(-\zeta\xi)\,\psi(\xi)\,d\xi \tag{19a}$$

where, $\chi(\zeta) = \zeta^2 j(F(\zeta))/ab^2$ and $\psi(\xi) = 2\varphi\left(\xi^{2/3}\right)/3\xi$

It is clear from Eq. (19a) that the function $\chi(\zeta)$ or subsequently $j(F)$ is the Laplace transform of the function $\psi(\xi)$ or subsequently $\varphi(\Phi)$. The inverse Laplace transform of Eq. (19a) gives the exact solution of $\psi(\xi)$ or subsequently $\varphi(\Phi)$ which is given as:

$$\psi(\xi) = \int_{\varepsilon-i\infty}^{\varepsilon+i\infty}\exp(\zeta\xi)\,\chi(\zeta)\,d\zeta \tag{20a}$$

References

[1] O. Richardson, On the Negative Radiation from Hot Platinum .., Univ. Press, Cambridge, 1901, http://www.worldcat.org/title/on-the-negative-radiation-from-hot-platinum/oclc/644310491. (Accessed 18 July 2018).

[2] A. Einstein, Über einen die Erzeugung und Verwandlung des Lichtes betreffenden heuristischen Gesichtspunkt, Ann. Phys. 322 (1905) 132–148.

[3] Josef Hölzl, Franz K. Schulte, Work function of metals, in: Solid Surface Physics, in: Springer Tracts in Modern Physics, vol. 85, 1979, pp. 1–150 (Chapter 1).

[4] I. Langmuir, The relation between contact potentials and electrochemical action, Trans. Am. Electrochem. Soc. 29 (125–180), 84.

[5] S. Seely, Work function and temperature, Phys. Rev. 59 (1941) 75–78.

[6] S. Halas, 100 years of work function, Mater. Sci. Pol. 24 (2006) 951–966.

[7] T. Durakiewicz, J. Sikora, S. Halas, Work function variations of incandescent filaments during self-cooling in vacuum, Vacuum 80 (2006) 894–898.

[8] S. Halas, T. Durakiewicz, Is work function a surface or a bulk property?, Vacuum 85 (2010) 486–488.

[9] S. Halas, T. Durakiewicz, P. Mackiewicz, Temperature-dependent work function shifts of hydrogenated/deuteriated palladium: a new theoretical explanation, Surf. Sci. 555 (2004) 43–50.

[10] V.A. Korol'kov, Temperature dependence of the work function of metals and binary alloys, Inorg. Mater. 37 (2001) 567–672.

[11] H. Lu, Z. Liu, X. Yan, D. Li, L. Parent, H. Tian, Electron work function-a promising guiding parameter for material design, Sci. Rep. 6 (2016) 1–11.

[12] I. Brodie, S.H. Chou, H. Yuan, A general phenomenological model for work function, Surf. Sci. 625 (2014) 112–118.

[13] D.K. De, O.C. Olawole, A three-dimensional model for thermionic emission from graphene and carbon nanotube, J. Phys. Commun. 3 (2019).

[14] O.C. Olawole, D.K. De, S.O. Oyedepo, F.I. Ezema, Mathematical models for thermionic emission current density of graphene emitter, Sci. Rep. 11 (2021) 22503.

[15] D.K. De, O.C. Olawole, Modified Richardson-Dushman equation and modeling thermionic emission from monolayer graphene, in: Proc. SPIE - Int. Soc. Opt. Eng., 2016.

[16] R. Rahemi, D. Li, Variation in electron work function with temperature and its effect on the Young's modulus of metals, Scr. Mater. 99 (2015) 41–44.

[17] H. Lu, D. Li, Correlation between the electron work function of metals and their bulk moduli, thermal expansion and heat capacity via the Lennard–Jones potential, Phys. Status Solidi 251 (2014) 815–820.

[18] G. Hua, D. Li, Generic relation between the electron work function and Young's modulus of metals, Appl. Phys. Lett. 99 (2011).

[19] X.C. Huang, H. Lu, H.B. He, X.G. Yan, D.Y. Li, Correlation between the wear resistance of Cu-Ni alloy and its electron work function 95 (2015) 3896–3909.

[20] Y. Li, D.Y. Li, Experimental studies on relationships between the electron work function, adhesion, and friction for 3d transition metals, J. Appl. Phys. 95 (2004) 7961.

[21] L. Guo, G. Hua, B. Yang, H. Lu, L. Qiao, X. Yan, D. Li, Electron work functions of ferrite and austenite phases in a duplex stainless steel and their adhesive forces with AFM silicon probe, Sci. Rep. 6 (2016) 20660.

[22] K.K. Kalazhokov, A.S. Gonov, Z.K. Kalazhokov, Calculation of single crystal face surface energy through its.., INIS, Metally (Mosk.) 28 (1996) 53–55, https://inis.iaea.org/search/search.aspx?orig_q=RN:28011965. (Accessed 31 July 2022).

[23] G. Hua, D. Li, Electron work function: a novel probe for toughness, Phys. Chem. Chem. Phys. 18 (2016) 4753–4759.

[24] S. Ogata, J. Li, Toughness scale from first principles, J. Appl. Phys. 106 (2009) 113534.

[25] X.C. Huang, H. Lu, D.Y. Li, Understanding the corrosion behavior of isomorphous Cu–Ni alloy from its electron work function, Mater. Chem. Phys. 173 (2016) 238–245.

[26] N.D. Lang, W. Kohn, Theory of metal surfaces: work function, Phys. Rev. B 3 (1971) 1215–1223.

[27] M. Yoshitake, Work Function and Band Alignment of Electrode Materials, 2021.

[28] D. Sinha, J.U. Lee, Ideal graphene/silicon Schottky junction diodes, Nano Lett. 14 (2014) 4660–4664.

[29] Y. Liu, H. Xiao, I. William A. Goddard, Schottky-barrier-free contacts with two-dimensional semiconductors by surface-engineered MXenes, J. Am. Chem. Soc. 138 (49) (2016) 15853–15856.

[30] X. Li, W. Cai, J. An, S. Kim, J. Nah, D. Yang, R. Piner, A. Velamakanni, I. Jung, E. Tutuc, S.K. Banerjee, L. Colombo, R.S. Ruoff, Large-area synthesis of high-quality and uniform graphene films on copper foils, Science 324 (2009) 1312–1314.

[31] F.V. Kusmartsev, W.M. Wu, M.P. Pierpoint, K.C. Yung, Application of graphene within optoelectronic devices and transistors, http://arxiv.org/abs/1406.0809, 2014. (Accessed 30 November 2016).

[32] D. Jariwala, V.K. Sangwan, L.J. Lauhon, T.J. Marks, C. Mark, Carbon nanomaterials for electronics, optoelectronics, photovoltaics, and sensing, (n.d.) 1–105.

[33] N.M. Nurazzi, N. Abdullah, S.Z.N. Demon, N.A. Halim, A.F.M. Azmi, V.F. Knight, I.S. Mohamad, The frontiers of functionalized graphene-based nanocomposites as chemical sensors, Nanotechnol. Rev. 10 (2021) 330–369.

[34] A. Kahn, Mater. Horiz. 3 (2016) 7–10.

[35] Y. Luo, Y. Tang, T.F. Chung, C.L. Tai, C.Y. Chen, J.R. Yang, D.Y. Li, Electron work function: an indicative parameter towards a novel material design methodology, Sci. Rep. 11 (2021) 11565.

[36] V. Junming Li, D.-I. Sabine Kunst, E. Kulke Gutachter, N. Koch, C.T. Koch, L. Liao, The performance characterization of carbazole/dibenzothiophene derivatives in modern OLEDs, 2016.

[37] F. Cleri, Energy band and vacuum level alignment at a semiconductor-molecule-metal interface, Appl. Phys. Lett. 92 (2008) 103112.

[38] P. Schindler, D.C. Riley, I. Bargatin, K. Sahasrabuddhe, J.W. Schwede, S. Sun, P. Pianetta, Z.X. Shen, R.T. Howe, N.A. Melosh, Surface photovoltage-induced ultralow work function material for thermionic energy converters, ACS Energy Lett. (2019) 2436–2443.

[39] S. Naghdi, K. Nešovic, G. Sánchez-Arriaga, H.Y. Song, S.W. Kim, K.Y. Rhee, V. Miškovic-Stankovic, The effect of cesium dopant on APCVD graphene coating on copper, J. Mater. Res. Technol. 9 (2020) 9798–9812.

[40] J.-H. Lee, I. Bargatin, B.K. Vancil, T.O. Gwinn, R. Maboudian, N.A. Melosh, R.T. Howe, Microfabricated thermally isolated low work-function emitter, J. Microelectromech. Syst. 23 (2014) 1182–1187.

[41] J.-H. Lee, I. Bargatin, N.A. Melosh, R.T. Howe, Optimal emitter-collector gap for thermionic energy converters, Appl. Phys. Lett. 100 (2012) 173904.

[42] Y. Zhou, C. Fuentes-Hernandez, J. Shim, J. Meyer, A.J. Giordano, H. Li, P. Winget, T. Papadopoulos, H. Cheun, J. Kim, M. Fenoll, A. Dindar, W. Haske, E. Najafabadi, T.M. Khan, H. Sojoudi, S. Barlow, S. Graham, J.-L. Brédas, S.R. Marder, A. Kahn, B. Kippelen, A universal method to produce low–work function electrodes for organic electronics, Science 336 (2012).

[43] L. Lindell, A. Burquel, F.L.E. Jakobsson, V. Lemaur, M. Berggren, R. Lazzaroni, J. Cornil, W.R. Salaneck, X. Crispin, Transparent, plastic, low-work-function poly(3,4-ethylenedioxythiophene) electrodes, Chem. Mater. 18 (2006) 4246–4252.

[44] A.L. Dadlani, P. Schindler, M. Logar, S.P. Walch, F.B. Prinz, Energy states of ligand capped Ag nanoparticles: relating surface plasmon resonance to work function, J. Phys. Chem. C 118 (2014) 24827–24832.

[45] S. Watanabe, T. Watanabe, K. Ito, N. Miyakawa, S. Ito, H. Hosono, S. Mikoshiba, Secondary electron emission and glow discharge properties of 12CaO·7Al2O3 electride for fluorescent lamp applications, http://www.tandfonline.com/action/journalInformation?show=aimsScope&journalCode=tsta20#.VmBmuzZFCUk, 2011.

[46] J.P. Snapp, J.-H. Lee, J. Provine, I. Bargatin, R. Maboudian, T.H. Lee, R.T. Howe, Sidewall silicon carbide emitters for terahertz vacuum electronics, in: 2012 Solid-State, Actuators, Microsystems Work. Tech. Dig., Transducer Research Foundation, San Diego, 2012, pp. 336–338.

[47] R.K. Barik, A. Bera, R.S. Raju, A.K. Tanwar, I.K. Baek, S.H. Min, O.J. Kwon, M.A. Sattorov, K.W. Lee, G.S. Park, Development of alloy-film coated dispenser cathode for terahertz vacuum electron devices application, Appl. Surf. Sci. 276 (2013) 817–822.

[48] J. Voss, A. Vojvodic, S.H. Chou, R.T. Howe, F. Abild-Pedersen, Inherent enhancement of electronic emission from hexaboride heterostructure, Phys. Rev. Appl. 2 (2014).

[49] M. Trenary, Surface science studies of metal hexaborides, Sci. Technol. Adv. Mater. 13 (2012) 023002.

[50] S. Naghdi, H.Y. Song, A. Várez, K.Y. Rhee, S.W. Kim, Engineering the electrical and optical properties of graphene oxide via simultaneous alkali metal doping and thermal annealing, J. Mater. Res. Technol. 9 (2020) 15824–15837.

[51] H.S. Devi, T.D. Singh, H.P. Singh, Optically understanding the dependence of catalysis kinetics on work function of nanocatalyst, Bull. Mater. Sci. 40 (2017) 163–170.

[52] Y. Pan, X. Shen, M.A. Holly, L. Yao, D. Wu, A. Bentalib, J. Yang, J. Zeng, Z. Peng, Oscillation of work function during reducible metal oxide catalysis and correlation with the activity property, ChemCatChem 12 (2020) 85–89.

[53] D. Hohertz, J. Gao, How electrode work function affects doping and electroluminescence of polymer light-emitting electrochemical cells, Adv. Mater. 20 (2008) 3298–3302.

[54] S. Biswas, P. Decorse, H. Kim, P. Lang, Organic planar diode with Cu electrode via modification of the metal surface by SAM of fluorobiphenyl based thiol, Appl. Surf. Sci. 558 (2021) 149794.

[55] E.S. Park, D.Y. Kim, J.H. Lee, J.U. Hwang, Y.S. Song, K.H. Park, H.J. Choi, Optical and electrical properties of amorphous alloy metal mesh for transparent flexible electrodes, Appl. Surf. Sci. 547 (2021) 149109.

[56] W. Li, D.Y. Li, Variations of work function and corrosion behaviors of deformed copper surfaces, Appl. Surf. Sci. 240 (2005) 388–395.

[57] M. Ganesan, C.C. Liu, S. Pandiyarajan, C.T. Lee, H.C. Chuang, Post-supercritical CO2 electrodeposition approach for Ni-Cu alloy fabrication: an innovative eco-friendly strategy for high-performance corrosion resistance with durability, Appl. Surf. Sci. 577 (2022) 151955.

[58] D.Y. Li, L. Guo, L. Li, H. Lu, Electron work function - a probe for interfacial diagnosis, Sci. Rep. 7 (2017).

[59] J. Pelletier, C. Pomot, Work function of sintered lanthanum hexaboride, Appl. Phys. Lett. 34 (1979) 249–251.

[60] P.L. Kanitkar, C.V. Dharmadhikari, D.S. Joag, V.N. Shukla, Field emission studies of the lanthanum hexaboride/tungsten system, 1976.

[61] W.B. Nottingham, Thermionic emission from tungsten and thoriated tungsten filaments, Phys. Rev. 49 (1936) 78–97.

[62] A. King, Photoelectric and thermionic investigations of thoriated tungsten surfaces, Phys. Rev. 53 (1938) 570–577.

[63] A. Sillero, D. Ortega, E. Muñoz-Serrano, E. Casado, An experimental study of thoriated tungsten cathodes operating at different current intensities in an atmospheric-pressure plasma torch, J. Phys. D, Appl. Phys. 43 (2010) 18.

[64] A. Bergner, M. Westermeier, C. Ruhrmann, P. Awakowicz, J. Mentel, Temperature measurements at thoriated tungsten electrodes in a model lamp and their interpretation by numerical simulation, J. Phys. D, Appl. Phys. 44 (2011) 15.

[65] H. Kawano, Effective work functions for ionic and electronic emissions from mono- and polycrystalline surfaces, Prog. Surf. Sci. 83 (2008) 1–165.

[66] H.J. Kreuzer, S.H. Payne, Theories of the adsorption-desorption kinetics on homogeneous surfaces, Stud. Surf. Sci. Catal. 104 (1997) 153–200.

[67] K. Wandelt, J.E. Hulse, Xenon adsorption on palladium. I. The homogeneous (110), (100), and (111) surfaces, J. Chem. Phys. 80 (1983) 1340–1352.

[68] C. Park, H.M. Kramer, E. Bauer, Distinct binding states in adsorption on a homogeneous surface: Te on W(100), Surf. Sci. 116 (1982) 456–466.

[69] H. Kawano, Effective work functions of the elements: database, most probable value, previously recommended value, polycrystalline thermionic contrast, change at critical temperature, anisotropic dependence sequence, particle size dependence, Prog. Surf. Sci. 97 (2022) 100583.

[70] G.F. Cerofolini, Adsorption and surface heterogeneity, Surf. Sci. 24 (1971) 391–403.
[71] C. Herring, M.H. Nichols, Thermionic emission, Rev. Mod. Phys. 21 (1949) 185–270.
[72] B.J. Hopkins, S. Usami, The surface potential of hydrogen on tungsten (100), (110) and (112) single crystal surfaces, Surf. Sci. 23 (1970) 423–426.
[73] B.J. Hopkins, K.R. Pender, The work function of a (110) oriented tungsten single-crystal face, Br. J. Appl. Phys. 17 (1966) 281.
[74] S. Naghdi, G. Sanchez-Arriaga, K.Y. Rhee, Tuning the work function of graphene toward application as anode and cathode, J. Alloys Compd. 805 (2019) 1117–1134.
[75] H. Luo, X. Zhou, C. Ellingford, Y. Zhang, S. Chen, K. Zhou, D. Zhang, C.R. Bowen, C. Wan, Interface design for high energy density polymer nanocomposites, Chem. Soc. Rev. 48 (2019) 4424–4465.
[76] X. Wang, J. Dan, Z. Hu, J.F. Leong, Q. Zhang, Z. Qin, S. Li, J. Lu, S.J. Pennycook, W. Sun, C.H. Sow, Defect heterogeneity in monolayer WS2 unveiled by work function variance, Chem. Mater. 31 (2019) 7970–7978.
[77] G.F. Rempfer, O.H. Griffith, The resolution photoelectron with UV, X-ray, and synchrotron excitation sources, Ultramicroscopy 27 (1989) 273–300.
[78] K.F. Mak, C. Lee, J. Hone, J. Shan, T.F. Heinz, Atomically thin MoS2: a new direct-gap semiconductor, Phys. Rev. Lett. 105 (2010).
[79] V.V. Afanas'Ev, A. Stesmans, Internal photoemission at interfaces of high-κ insulators with semiconductors and metals, J. Appl. Phys. 102 (2007) 081301.
[80] M.G. Helander, M.T. Greiner, Z.B. Wang, Z.H. Lu, Pitfalls in measuring work function using photoelectron spectroscopy, Appl. Surf. Sci. 256 (2010) 2602–2605.
[81] S.J. Altenburg, R. Berndt, Local work function and STM tip-induced distortion of graphene on Ir(111), New J. Phys. 16 (2014) 053036.
[82] H.C. Wen, R. Choi, G.A. Brown, T. Böscke, K. Matthews, H.R. Harris, K. Choi, H.N. Alshareef, H. Luan, G. Bersuker, P. Majhi, D.L. Kwong, B.H. Lee, Comparison of effective work function extraction methods using capacitance and current measurement techniques, IEEE Electron Device Lett. 27 (2006) 598–601.
[83] KP Technology Ltd, (n.d.), http://www.kelvinprobe.info/introduction.htm. (Accessed 30 July 2022).
[84] J. Hölzl, F.K. Schulte, Work function of metals, in: STMP, vol. 85, 1979, p. 1.
[85] P.A. Anderson, A new technique for preparing monocrystalline metal surfaces for work function study. The work function of Ag(100), Phys. Rev. 59 (1941) 1034.
[86] M. Rohwerder, Passivity of metals and the Kelvin probe technique, Encycl. Interfacial Chem. Surf. Sci. Electrochem. (2018) 414–422.
[87] R. Mehrotra, J. Mahanty, Free electron contribution to the workfunction of metals, J. Phys. C, Solid State Phys. 11 (1978) 2061–2064.
[88] M. Weinert, R.E. Watson, Contributions to the work function of crystals, Phys. Rev. B 29 (1984) 3001–3008.
[89] J.R. Smith, Self-consistent many-electron theory of electron work functions and surface potential characteristics for selected metals, Phys. Rev. 181 (1969) 522.
[90] C.A. Utreras-Diaz, Metallic surfaces in the Thomas–Fermi–von Weizsäcker approach: self-consistent solution, Phys. Rev. B 36 (1987) 1785–1788.
[91] J.P. Perdew, Y. Wang, Jellium work function for all electron densities, Phys. Rev. B 38 (1988) 12228–12232.
[92] J.P. Perdew, H.Q. Tran, E.D. Smith, Stabilized jellium: structureless pseudopotential model for the cohesive and surface properties of metals, Phys. Rev. B 42 (1990) 11627–11636.
[93] H.B. Shore, J.H. Rose, Theory of ideal metals, Phys. Rev. Lett. 66 (1991) 2519–2522.
[94] H.L. Skriver, N.M. Rosengaard, Surface energy and work function of elemental metals, Phys. Rev. B 46 (1992) 7157–7168.
[95] M. Methfessel, D. Hennig, M. Scheffler, Trends of the surface relaxations, surface energies, and work functions of the 4d transition metals, Phys. Rev. B 46 (1992) 4816–4829.
[96] K.F. Wojciechowski, Quantum size effect in the work function of jellium slabs confined by a finite well of thickness-dependent depth, Phys. Rev. B 60 (1999) 9202.
[97] C.J. Fall, N. Binggeli, A. Baldereschi, Deriving accurate work functions from thin-slab calculations, J. Phys. Condens. Matter 11 (1999) 2689–2696.
[98] S. Halas, T. Durakiewicz, Work functions of elements expressed in terms of the Fermi energy and the density of free electrons, 1998.
[99] I. Brodie, Uncertainty, topography, and work function, Phys. Rev. B 51 (1995) 13660–13668.
[100] T. Durakiewicz, A. Arko, J.J. Joyce, D.P. Moore, S. Halas, Electronic work-function calculations of polycrystalline metal surfaces revisited, Phys. Rev. B, Condens. Matter Mater. Phys. 64 (2001) 045101.
[101] S. Kajita, T. Nakayama, J. Yamauchi, Density functional calculation of work function using charged slab systems, J. Phys. Conf. Ser. 29 (2006) 120–123.
[102] Y. Ikuno, K. Kusakabe, A determination method of the work function using the slab model with a first-principles electronic structure calculation, E-J. Surf. Sci. Nanotechnol. 6 (2008) 103–106.
[103] R. Jacobs, J. Booske, D. Morgan, Understanding and controlling the work function of perovskite oxides using density functional theory, Adv. Funct. Mater. 26 (2016) 5471–5482.
[104] Z. Zhong, P. Hansmann, Tuning the work function in transition metal oxides and their heterostructures, Phys. Rev. B 93 (2016) 235116.
[105] S. De Waele, K. Lejaeghere, M. Sluydts, S. Cottenier, Error estimates for density-functional theory predictions of surface energy and work function, Phys. Rev. B 94 (2016) 235418.
[106] R. Jacobs, D. Morgan, J. Booske, Work function and surface stability of tungsten-based thermionic electron emission cathodes, APL Mater. 5 (2017) 116105.
[107] H.A. Tahini, X. Tan, S.C. Smith, The origin of low workfunctions in OH terminated MXenes, Nanoscale 9 (2017) 7016–7020.
[108] J. Chrzanowski, B. Bieg, Precise, semi-empirical equation for the work function, Appl. Surf. Sci. 461 (2018) 83–87.
[109] B. Bieg, J. Chrzanowski, Electron chemical potential in the context of unconventional quantum model, Appl. Surf. Sci. 461 (2018) 78–82.
[110] Q. Zhou, X. Liu, T. Maxwell, B. Vancil, T.J. Balk, M.J. Beck, BaxScyOz on W (0 0 1), (1 1 0), and (1 1 2) in scandate cathodes: connecting to experiment via μO and equilibrium crystal shape, Appl. Surf. Sci. 458 (2018) 827–838.
[111] S.A. Chambers, P.V. Sushko, Influence of crystalline order and defects on the absolute work functions and electron affinities of Ti O2 - and SrO-terminated n-SrTi O3(001), Phys. Rev. Mater. 3 (2019) 125803.
[112] R. Tran, X.G. Li, J.H. Montoya, D. Winston, K.A. Persson, S.P. Ong, Anisotropic work function of elemental crystals, Surf. Sci. 687 (2019) 48–55.
[113] J. Chrzanowski, M. Matuszak, The double dipole layer and work function of metals, Appl. Surf. Sci. 527 (2020).
[114] T. Ma, R. Jacobs, J. Booske, D. Morgan, Understanding the interplay of surface structure and work function in oxides: a case study on SrTiO3, APL Mater. 8 (2020) 071110.
[115] W. Hashimoto, Y. Tsuji, K. Yoshizawa, Optimization of work function via Bayesian machine learning combined with first-principles calculation, J. Phys. Chem. C 124 (2020) 9958–9970.
[116] O. Olubosede, O.M. Afolabi, R.S. Fayose, E.O. Oniya, A.C. Tomiwa, Comparison of calculated work function of metals using metallic plasma model with stabilized jellium, ab-initio approach and experimental values, Appl. Phys. Res. 3 (2011) 171–178.
[117] P. Schindler, E.R. Antoniuk, G. Cheon, Y. Zhu, E.J. Reed, Discovery of materials with extreme work functions by high-throughput density functional theory and machine learning, undefined (2020).
[118] T. Ma, R. Jacobs, J. Booske, D. Morgan, Work function trends and new low-work-function boride and nitride materials for electron emission applications, J. Phys. Chem. C 125 (2021) 17400–17410.
[119] R.H. Fowler, The analysis of photoelectric sensitivity curves for clean metals at various temperatures, Phys. Rev. 38 (1931) 45.
[120] Lee Alvin DuBridge, New Theories of the Photoelectric Effect, Google Books, (n.d.), https://books.google.com.ng/books/about/New_Theories_of_the_Photoelectric_Effect.html?id=KJfOAAAAMAAJ&redir_esc=y. (Accessed 4 August 2022).